A numerical consideration on edge effect of planar dipole phased arrays

Shoichiro Fukao Toru Sato Hiroshi Hojo Iwane Kimura and Susumu Kato

Reprinted from
RADIO SCIENCE
Volume 21 Number 1 January/February 1986

Radio Science, Volume 21, Number 1, Pages 1–12, January–February 1986

A numerical consideration on edge effect of planar dipole phased arrays

Shoichiro Fukao[1,2], *Toru Sato*[2], *Hiroshi Hojo*[1,3], *Iwane Kimura*,[1] *and Susumu Kato*[2]

(Received January 23, 1985; revised July 23, 1985; accepted August 5, 1985.)

The edge effect of planar phased hexagonal arrays is numerically investigated by comparing exact solutions of active impedance and array element pattern of finite arrays with those determined with infinite array approximation. The analysis incorporates the improved circuit theory, which has a higher accuracy than the electro-motive-force method. Considerations are also made for the edge effect on the total array pattern. It is found that the edge effect is in reverse proportion to array size. It can be neglected for arrays composed of more than 200 elements, for which the array pattern can be well approximated by the product of the array factor and array element pattern of an infinite array.

1. INTRODUCTION

A planar phased array with an aperture of 10^4–10^5 m^2 is the indispensable component for the VHF-band MST (mesosphere-stratosphere-troposphere) radars. This type of radar which operates near 50 MHz is capable of observing the various dynamical processes occurring in the middle atmosphere (altitude range 10–100 km) [e.g., *Balsley and Gage*, 1980].

The arrays are composed of a large number of linear antennas such as dipole, coaxial colinear or Yagi. They are required to have a high-gain main lobe with extremely low sidelobes in order to suppress ground clutter as well as low-elevation intense tropospheric scattering. Therefore, the precisest evaluation of directivity is quite important in designing the pertinent large arrays.

The performance characteristics of large arrays, namely, array element pattern, and active impedance and total array pattern variations with beam scan angle, are generally analyzed with the infinite array approximation that assumes the arrays to have the infinite extent with uniformly spaced identical elements [*Stark*, 1966]. Such approximation appears to provide mutual coupling effects very simply, that are otherwise very complicate to analyze. However, the number of elements is not infinite but finite in actual arrays, and the individual element properties differ from that of the infinite array, especially, near the edge of the array [e.g., *Diamond*, 1965; *Hansen*, 1966].

Edge effect of planar phased array has been principally investigated by comparing calculated or measured performance characteristics of a finite array with theoretical ones determined with the aid of infinite array approximation [e.g., *Hansen*, 1966]. However, even the most comprehensive computer investigation by *Diamond* [1965] has been restricted either to the performance of the center element of a large rectangular-grid array or to rather small size ones of the same type of arrays with up to 100 elements due to the computer machine limitation at that time. General feature of the edge effect of the rectangular-grid dipole arrays is fairly well understood by Diamond's work, but it is felt that still further investigation should be undertaken in order to comply with growing demand for optimized MST radar arrays with grids other than the rectangular one [*Kato et al.*, 1984].

The present investigation will be an extension of the Diamond's work, in which exact solutions of the performance characteristics are compared with those subject to the infinite array approximation for arrays of various sizes with elements up to 300. The results given will be for only hexagonal arrays with half-wave dipoles arranged on triangular grids. This problem has been left unsolved despite its considerable practical interest.

The following analysis on finite arrays does not make the assumption of constant current to each element in the array. Instead, the currents driving individual elements are computed exactly by calculating the inverse of the impedance matrix, assuming that

[1]Department of Electrical Engineering, Kyoto University, Yoshida, Japan.

[2]Radio Atmospheric Science Center, Kyoto University, Uji, Japan.

[3]Now at NTT Electrical Communications Laboratories, Kanagawa, Japan.

Paper number 5S0649.
0048-6604/86/005S-0649$08.00

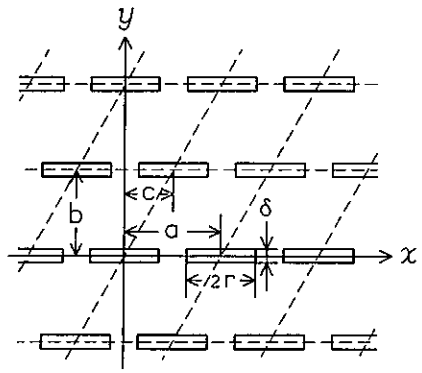

Fig. 1. Geometry of the infinite planar array with dipoles arranged on a general triangular grid. The dipoles are represented by equivalent thin sheets of width δ and length $2r(2r = \lambda/2; \lambda$ is wavelength).

each element is excited by a power supply of a constant voltage with an internal serial impedance, as is ordinarily the case in most arrays. Also, the analysis incorporates the improved circuit theory (ICT) [*Inagaki*, 1969], in which current distribution is approximated by a linear combination of more than one function. This method is known to be of greater accuracy than the ordinary electro-motive-force method used by *Diamond* [1965].

2. METHOD OF ANALYSIS

2.1. *Infinite array analysis*

In order to minimize the complexity of analysis, an infinite planar array with half-wave elements arranged periodically in a general triangular grid shown in Figure 1 is considered here. All elements are assumed to have equal current distribution. Here, we will follow the analysis presented by *Stark* [1966] for infinite planar dipole arrays over a perfectly conducting ground plane.

The current is assumed to flow uniformly in the lateral direction in an infinitely thin sheet of width δ, and approximated by a linear combination of the following two functions [*Inagaki*, 1969]:

$$K^1 = \frac{I_0^1}{\delta} \cos kx \tag{1a}$$

$$K^2 = \frac{I_0^2}{\delta}(1 - \sin k|x|) \tag{1b}$$

$$|x| \le \lambda/4 \qquad |y| \le \delta/2$$

where $k = 2\pi/\lambda$ is the wave number, λ is the wavelength, and I_0^1 and I_0^2 are the currents at the center of each element. The infinitely thin element of width δ is equivalent to a cylindrical element of radius $(d=)$ $\delta/4.48$ [*Uda and Mushiake*, 1954].

The spatial Fourier harmonics for the respective current functions, $K_{\mu\nu}^1$ and $K_{\mu\nu}^2$, are expressed as follows:

$$K_{\mu\nu}^1 = \frac{1}{ab}\int_{-\lambda/4}^{\lambda/4}\int_{-\delta/2}^{\delta/2} K^1 e^{i\beta_\mu x} e^{jh_{\mu\nu}y}\, dx\, dy$$

$$= \frac{2I_0^1}{ab}\cdot\frac{\sin(h_{\mu\nu}\delta/2)}{h_{\mu\nu}\delta/2}\cdot\frac{k\cos(\beta_\mu\lambda/4)}{k^2-\beta_\mu^2} \tag{2a}$$

$$K_{\mu\nu}^2 = \frac{2I_0^2}{ab}\cdot\frac{\sin(h_{\mu\nu}\delta/2)}{h_{\mu\nu}\delta/2}$$

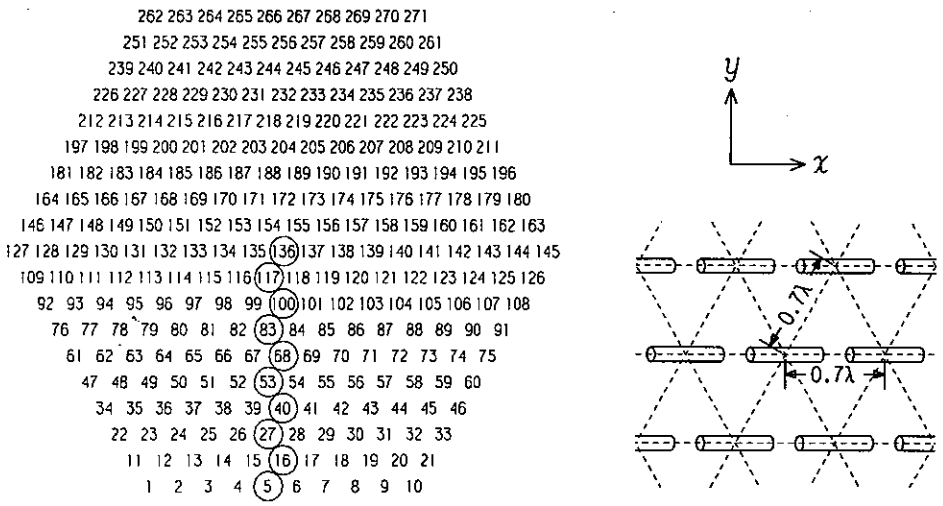

Fig. 2. The finite hexagonal array composed of 271 elements which are arranged on equilateral triangular grids with element spacing of 0.7λ (λ is wavelength). Consecutive numbers are put in the element positions. Encircled elements will be discussed later.

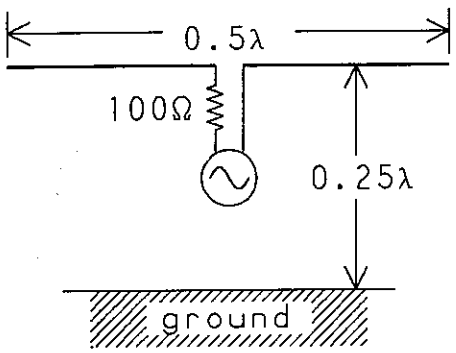

Fig. 3. Geometry of the half-wave dipoles.

$$\cdot \left\{ \frac{\lambda}{4} \frac{\sin (h_{\mu\nu} \lambda/4)}{h_{\mu\nu} \lambda/4} + \frac{h_{\mu\nu} \sin (h_{\mu\nu} \lambda/4) - k}{k^2 - h_{\mu\nu}^2} \right\} \tag{2b}$$

where β_μ and $h_{\mu\nu}$, the wave numbers in x and y directions, respectively, are given by

$$\beta_\mu = k \cos \theta_x + 2\pi\mu/a$$

$$h_{\mu\nu} = k \cos \theta_y + 2\pi(\nu - \mu c/a)/b$$

for an antenna beam with angles of θ_x and θ_y relative to x and y axes, respectively.

The mutual impedance between current functions p and q is given by [*Stark*, 1966]

$$Z^{pq} = -\frac{ab\eta_0}{2} \sum_{\mu=-\infty}^{\infty} \sum_{\nu=-\infty}^{\infty} \frac{\beta_\mu^2 - k^2}{k\gamma_{\mu\nu}} \cdot \frac{K_{\mu\nu}^p K_{\mu\nu}^q}{I_0^p I_0^q} (1 - e^{-2j\gamma_{\mu\nu}H}) \tag{3}$$

$$p, q = 1, 2$$

where η_0 is the characteristic impedance of free space ($=376.73\ \Omega$), H is the element height from the perfectly conducting ground plane, and

$$\gamma_{\mu\nu} = (k^2 - \beta_\mu^2 - h_{\mu\nu}^2)^{1/2}$$

The current functions can be determined by solving the following circuit equation:

$$\begin{bmatrix} Z^{11} + Z_g & Z^{12} + Z_g \\ Z^{21} + Z_g & Z^{22} + Z_g \end{bmatrix} \begin{bmatrix} I_0^1 \\ I_0^2 \end{bmatrix} = \begin{bmatrix} V_0 \\ V_0 \end{bmatrix} \tag{4}$$

where V_0 and Z_g are the constant unit voltage and the internal serial impedance of the power supply fed to each antenna element, respectively. Using I_0^1 and I_0^2, the active impedance and the array element pattern are given as follows:

$$Z_a = \frac{V_0}{I_0^1 + I_0^2} - Z_g \tag{5}$$

$$F_e(\theta_x) = \sum_{p=1}^{2} I_0^p f_a^p(\theta_x) \tag{6}$$

where $f_a^p(\theta_x)$ denotes the array element pattern owing to each current function $K^p (p = 1, 2)$.

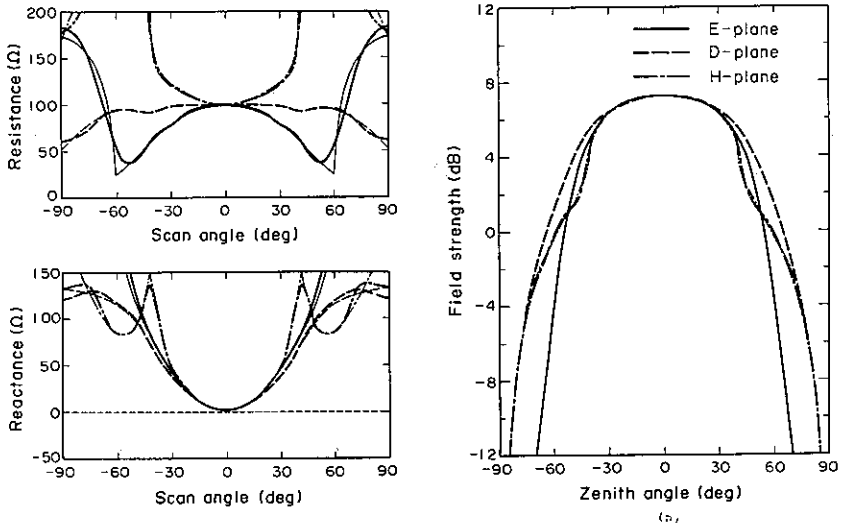

Fig. 4. (*a*) Active impedance (resistance and reactance components in the top and bottom, respectively) and (*b*) array element pattern compared between element in the infinite array (thin lines) and the 136th element situated at the center of the finite array of Figure 2 (thick lines). Field strength which is normalized to the radiation field of an isotropic antenna matched to the feed line is given against zenith angle. The solid and dashed curves and chain are for the directions of $E(x\text{-}z)$, D (diagonal; 45° with respect to the x axis) and $H(y\text{-}z)$ planes, respectively.

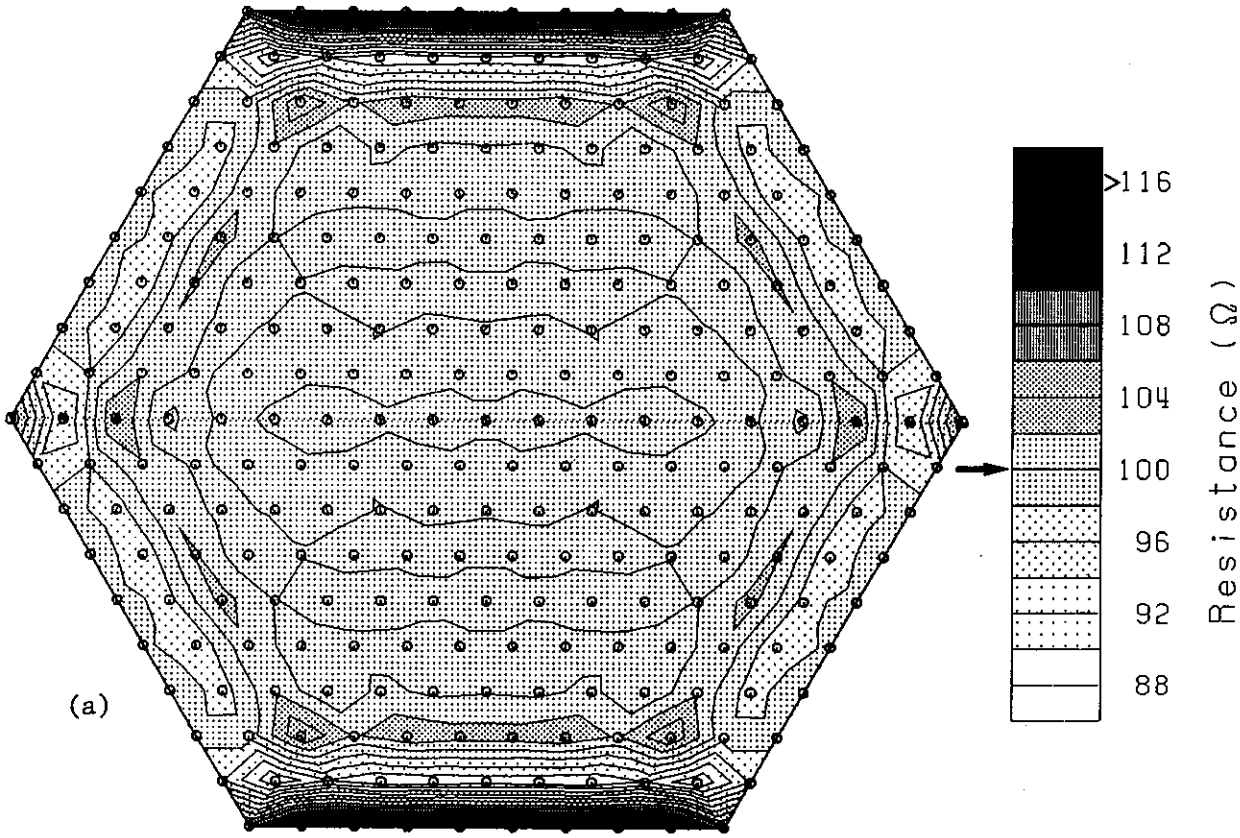

Fig. 5. Spatial variation of (*a*) active resistance, (*b*) active reactance and (*c*) array element gain shown in the form of a contour map. The element positions are shown by small circles, and the dipole direction is parallel to the bottom edge of the array. The arrow put on the contour scale on the right-hand side of each map indicates the values for the infinite array element.

2.2. *Finite array analysis*

For a finite array, the current distributions on individual elements are not identical due to the edge effect, and the circuit equation (4) should be solved for all, i.e. $2 \times L$ (L is number of elements), current functions.

The same current functions as (1) are assumed on each element of the finite array:

$$I_l^1 = I_{l0}^1 \cos kx \tag{7a}$$

$$I_l^2 = I_{l0}^2(1 - \sin k|x|) \tag{7b}$$

$$|x| \le \lambda/4 \qquad |y| \le d/2 \qquad l = 1, 2, \cdots, L$$

where d is the dipole radius.

The mutual impedance between dipoles whose centers are placed at the positions $P_1(x_m, y_m)$ and $P_2(x_n, y_n)$, respectively, is given by the following integral [*Inagaki*, 1969];

$$Z_{mn}^{pq} = -\int_{-\lambda/4}^{\lambda/4}\int_{-\lambda/4}^{\lambda/4} G(\xi_m, \xi_n)\frac{I_m^p I_n^q}{I_{m0}^p I_{n0}^q}\, d\xi_m\, d\xi_n \tag{8}$$

where $G(\xi_m, \xi_n)$ is the Green function given as

$$G(\xi_m, \xi_n) = -j\frac{k\eta_0}{4\pi}\left(1 + \frac{1}{k^2}\frac{\partial^2}{\partial \xi_n^2}\right)\frac{e^{-jk\rho}}{\rho}$$

$$\rho = \{(x_m + \xi_m - x_n - \xi_n)^2 + (y_m - y_n)^2\}^{1/2}$$

$$p, q = 1, 2 \qquad m, n = 1, 2, \cdots, L$$

When P_2 is represented by the relative coordinates (x_d, y_d) to P_1, ρ is rewritten as

$$\rho = \{(x_d + \xi_n - \xi_m)^2 + y_d^2\}^{1/2}$$

where

$$y_d = y_m - y_n \qquad m \ne n$$

$$y_d = d \qquad m = n$$

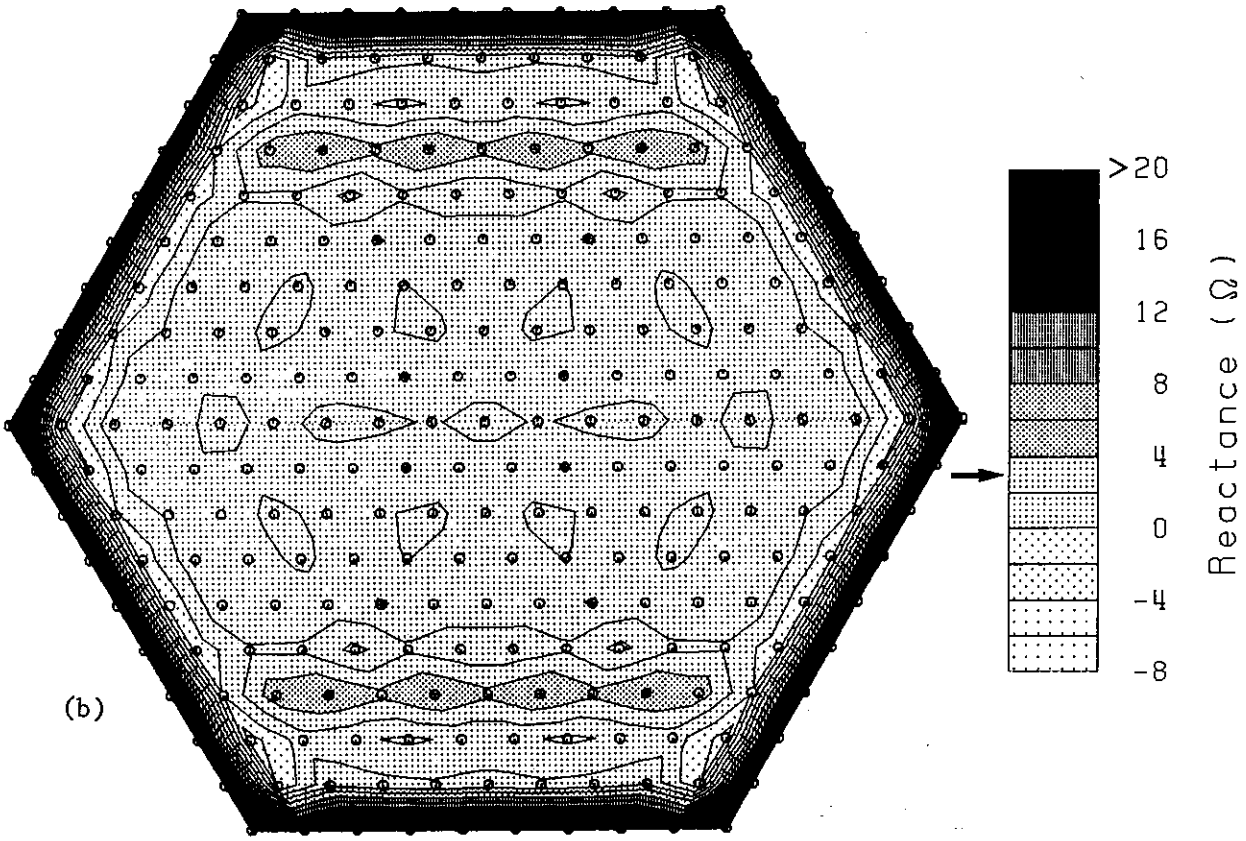

Fig. 5. (continued)

The double integrals of Z_{mn}^{pq} are changed to single integrals as follows (see Appendix for their derivation):

$$Z_{mn}^{11} = j\frac{\eta_0}{4\pi}\left\{S^{11}\left(\frac{\lambda}{2}\right) + S^{11}\left(-\frac{\lambda}{2}\right)\right\} \tag{9a}$$

$$S^{11}(\xi) = -\sin kx_d E_c(\xi) - \cos kx_d E_s(\xi)$$

$$Z_{mn}^{12} = j\frac{\eta_0}{4\pi}\left\{S^{12}\left(\frac{\lambda}{2}\right) - S^{12}\left(-\frac{\lambda}{2}\right)\right\} \tag{9b}$$

$$S^{12}(\xi) = E_E(\xi) + \cos kx_d\left\{E_C(\xi) + 2E_S\left(\frac{\xi}{2}\right)\right\}$$

$$+ \sin kx_d\left\{E_S(\xi) - 2E_C\left(\frac{\xi}{2}\right)\right\}$$

$$Z_{mn}^{22} = j\frac{\eta_0}{4\pi}\left\{S^{22}\left(\frac{\lambda}{2}\right) + S^{22}\left(-\frac{\lambda}{2}\right)\right\} \tag{9c}$$

$$S^{22}(\xi) = \sin kx_d\left\{E_C(\xi) - 4E_C\left(\frac{\xi}{2}\right)\right\}$$

$$- \cos kx_d\left\{E_S(\xi) - 4E_S\left(\frac{\xi}{2}\right)\right\}$$

$$-\frac{\xi}{|\xi|}E_E\left(\frac{\xi}{2}\right) + kx_d E_E(\xi) - E_L(\xi)$$

where

$$E_C(\xi) = \int_{x_d}^{x_d+\xi} g_0 \cos ku\, du \qquad E_S(\xi) = \int_{x_d}^{x_d+\xi} g_0 \sin ku\, du$$

$$E_E(\xi) = \int_{x_d}^{x_d+\xi} g_0\, du \qquad E_L(\xi) = \int_{x_d}^{x_d+\xi} kug_0\, du$$

and

$$g_0 = \frac{e^{-jk\rho_0}}{\rho_0} \qquad \rho_0 = (u^2 + y_d^2)^{1/2}$$

The circuit equation is given in the following matrix with mutual impedance $\tilde{Z}_{mn}^{pq}$ between one current function and the image of other current function due to the ground plane included as in the infinite array approximation (cf. (3)).

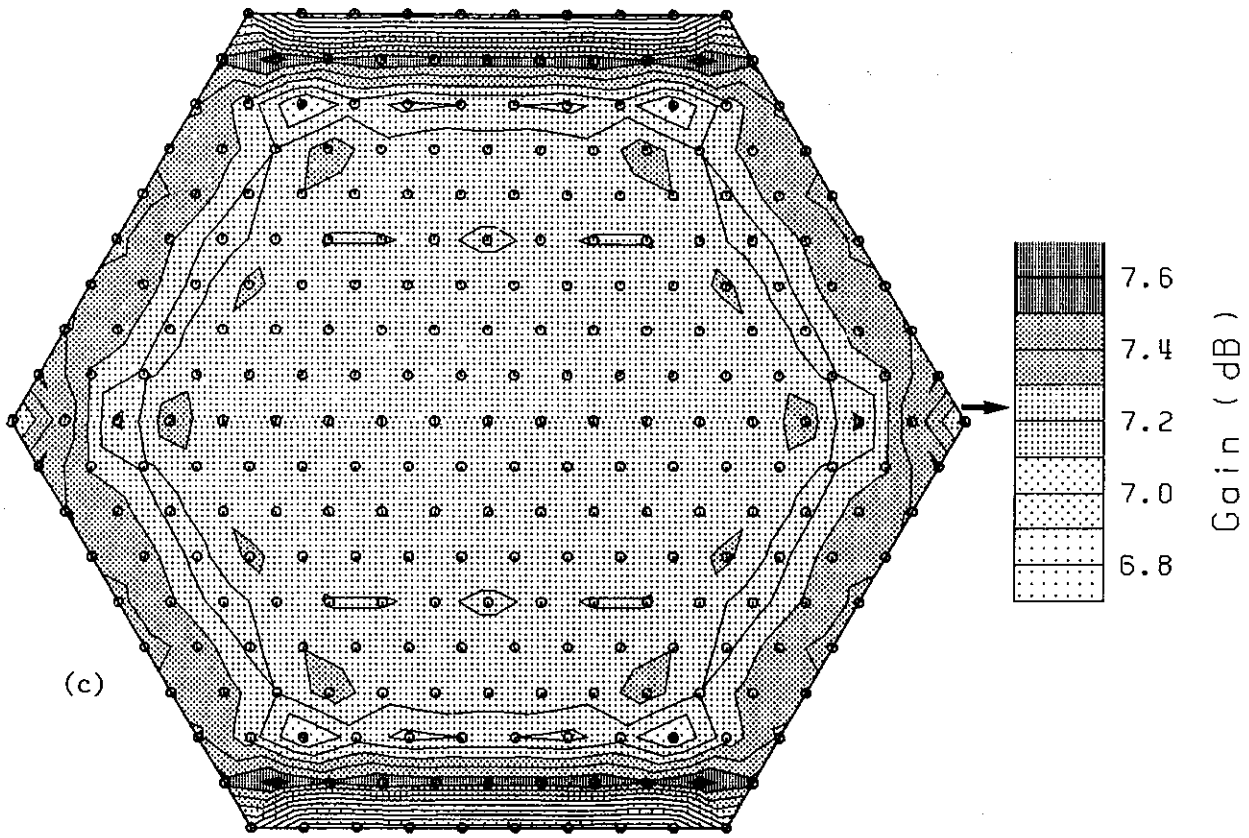

Fig. 5. (continued)

$$\sum_{q=1}^{2}\sum_{n=1}^{L}(Z_{mn}^{pq}-\tilde{Z}_{mn}^{pq}+\delta_{mn}Z_g)I_n^q=V_{m0} \tag{10}$$

$$\delta_{mn}=1 \qquad (m=n)$$

$$\delta_{mn}=0 \qquad (m\neq n)$$

$$p=1,2 \qquad m=1,2,\cdots,L$$

where V_{m0} and Z_g are the constant unit voltage and the internal serial impedance of the power supply to the mth element, which are respectively assumed to be identical for all elements, since that is the usual case in large arrays. $\tilde{Z}_{mn}^{pq}$ can be expressed in a manner similar to (9).

By solving (10), the active impedance and the array element pattern (exact solution) are given as follows:

$$Z_{al}=\frac{V_{l0}}{I_{l0}^1+I_{l0}^2}-Z_g \tag{11a}$$

$$F_{el}(\theta_x)=2j\sum_{m=1}^{L}\sum_{p=1}^{2}I_{m0}^p f^p(\theta_x)\sin(kH\cos\theta_z)\cdot e^{jk(x_m\cos\theta_x+y_m\cos\theta_y)} \tag{11b}$$

where θ_z is the zenith angle, and $f^p(\theta_x)$ is the element pattern due to the current function I_m^p. Only l'th element is excited and all other elements are passively terminated, when $F_{el}(\theta_x)$ is determined.

3. RESULTS

The maximum number of unknown current functions is restricted by the computer memory size, and we examine a few hexagonal arrays composed of up to 271 half-wave cylindrical dipoles which are arranged on the grid of an equilateral triangular as shown in Figure 2. The element spacing is 0.7λ. The dipole height (H) is $\lambda/4$, while the internal serial impedance (Z_g) is supposed to be 100 Ω (Figure 3). The dipole radius (or the equivalent radius, d) is chosen as $1.68\times10^{-3}\lambda$, sufficiently small compared with λ.

3.1. *Element properties at the array center*

The element properties for elements near the center of a finite array as large as that of 271 dipoles are expected to be similar to those of infinite array

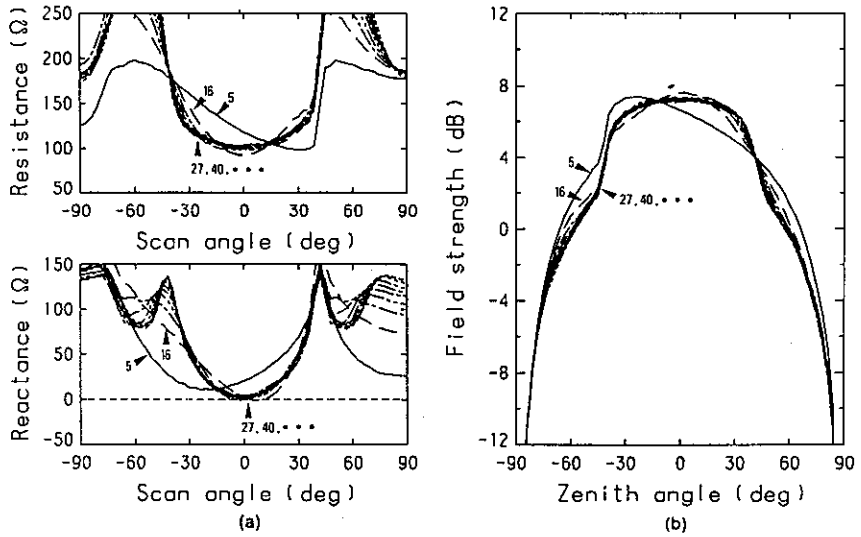

Fig. 6. (*a*) Active impedance and (*b*) array element pattern (*H* plane) for the ten elements encircled in Figure 2. They are shown by solid (5th) and dashed (16th) lines, one-point chain (27th), two-point chain (40th), etc. for the element order approaching the center from the edge of the array.

elements. Figure 4 compares active impedance and array element pattern of the infinite array element with those of the center element of the finite array for the case where the antenna beam is directed toward the zenith. The thin lines indicate the properties of the infinite array element, while the thick lines show those of the center element of the finite array. It is clearly shown in this figure that the element properties of the center element of the finite array are quite similar to those of the infinite array element.

3.2. *Spatial variation of element properties*

Element properties are expected to change from element to element in the finite array. Figure 5 shows active impedance and array element gain of each element in the finite array in the form of a contour map for the case where the antenna beam is directed to the zenith. The representation in this form is useful for showing an overall spatial variation within an array, but it should be noted that the contours are meaningful only at the element positions.

Active impedance and array element gain for the infinite array element are $100.0 + j2.6\ \Omega$ and 7.24 dB, respectively, as indicated by the arrows placed on the contour scales. Both active impedance and array element gain for elements inside the 3rd row from the array edge do not differ more than $\pm 2\ \Omega$ and ± 0.1 dB, respectively, from those of the infinite array element.

Difference of the exact element properties of the individual finite array elements from those of infinite array element is largest at the edge of the array, decreasing rapidly with approaching the center of the array. Generally, the edge elements have the active impedance between the value of the infinite array and that of the single isolated element, $109.0 + j74.0\ \Omega$. Therefore, it is considered that the edge effect is less significant for Yagi arrays than for dipole arrays discussed here, since the element properties of a single isolated element differ less from those of the infinite array element for multi-subelement antennas than for dipoles.

3.3. *Asymmetry of element properties*

The number of elements surrounding a specific element differs according to the element position in the finite array, which causes asymmetry of the element properties with respect to the zenith (or scan angles). The element properties in the *H* plane are shown in Figure 6 for the ten elements encircled in Figure 2. The largest asymmetry is seen at the 5th element situated at the array edge, and the elements inside the 27th element placed in the third row show the properties very similar to those near the array center.

In the half-wave-spaced rectangular-grid array of *Diamond* [1965], an edge effect of the order of 10% or more is observed in at least the outer 4 or 5 rows of elements. Effective aperture of a single element in his rectangular-grid array is 0.59 times that in the

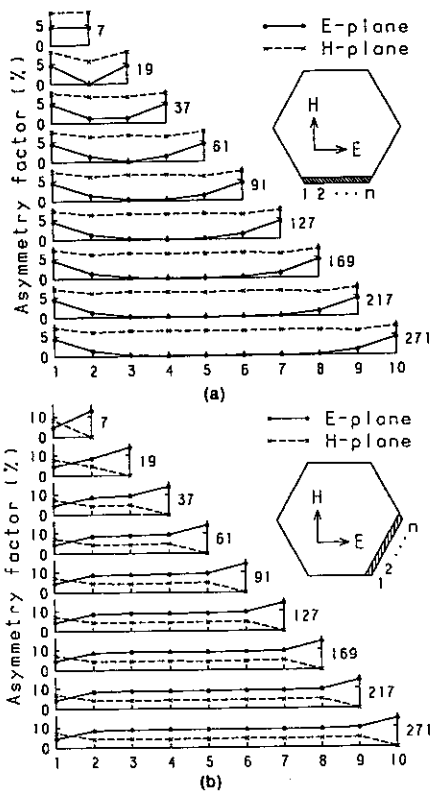

Fig. 7. Asymmetry of array element pattern at the edges of nine hexagonal arrays with different size. The ordinate is the asymmetry factor, while the abscissa is the element positions at the array edges indicated by shade. The top diagram is for the smallest hexagonal array with 2 edge elements, whereas the bottom one is for the array with 10 edge elements. The total number of elements is given on the right of each diagram. All elements are aligned parallel to the bottom edge in 7*a*, while they are at an angle of 60° with respect to the side edge in 7*b*. The values in the *E* and *H* planes are given by solid and broken lines, respectively.

present equilateral-triangular-grid array. Thus, the coupling between elements is tighter in the rectangular grid, so that the edge effect is observed further into the interior of the array in the rectangular grid than in the triangular one.

Next, the element patterns of the outermost array elements are investigated for various sizes of the similar hexagonal arrays. An "asymmetry factor" is defined as the ratio of asymmetric component of array element pattern to a symmetric one averaged over the zenith angle. The factor is obtained for the two different edge rows indicated by shade in the hexagonal arrays shown on the right of Figures 7*a* and 7*b*, respectively.

The asymmetry is most conspicuous on the corner of the array with the asymmetry factor of the order of 10%, whereas it is almost constant, being independent of the array size, for the elements inside the 3rd one from the corner. As expected, the element alignment in 7*a* gives a larger asymmetry in the *H* plane, while the asymmetry in the *E* plane is generally more conspicuous for the alignment in 7*b*.

3.4. *Deterioration of directivity*

The edge effect causes current distribution to differ among individual elements, which deteriorates directivity of the array. In Figure 8, a comparison of total array pattern is made between the exact solution and that determined with infinite array approximation for the hexagonal array composed of 271 elements. The antenna beam is directed 30° from the zenith.

There is virtually no significant difference in the main lobe. The difference between the two patterns appears only at the low elevation sidelobes, and is at

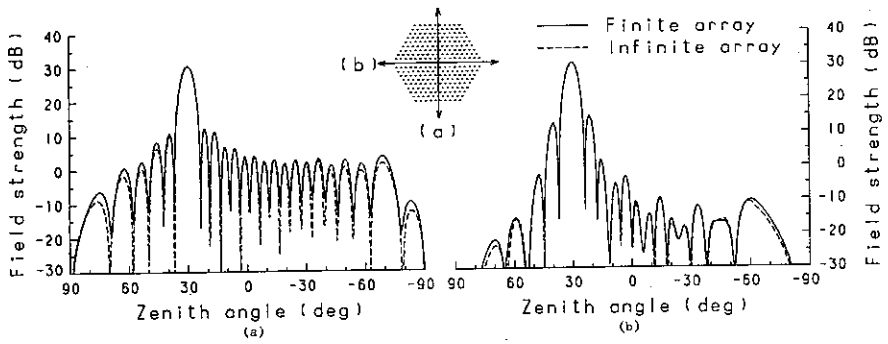

Fig. 8. Comparison of the total array pattern between the infinite and finite array analyses. The array pattern obtained by the finite array analysis is shown by the solid lines, while that obtained by the finite array analysis is given by the dashed lines. The array patterns in the *H* and *E* planes are, respectively, obtained along the vertical planes indicated by 8*a* and 8*b* in the hexagonal array of 271 elements shown near the center of the figure. The abscissa is the zenith angle, while the ordinate is the electric field intensity over the radiation field of the isotropic antenna in dB. (*a*) *H* plane and (*b*) *E* plane.

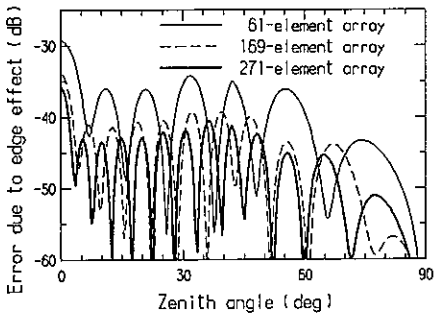

Fig. 9. Difference of the field intensity in the H plane between the exact solution and that obtained with infinite array approximation for three hexagonal arrays with different size. The difference is normalized to the main lobe field intensity of the respective arrays.

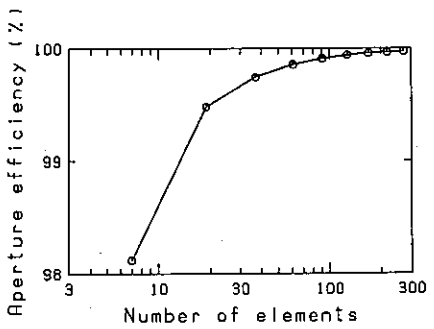

Fig. 11. The aperture efficiency of the array versus array size. The small circles show the calculated values for hexagonal arrays with elements of 7, 19, 37, 61, 91, 127, 169, 217, and 271, respectively.

most 2.5 dB. Therefore, the deterioration of array pattern due to the edge effect is considered to be quite small in large arrays such as the one with 271 elements investigated here.

3.5. *Edge effect versus array size*

As mentioned above, the edge effect appears most significantly at the outermost array elements. In general planar arrays, the total number of array elements increases proportionally to the square of array radius, while that of the outermost elements is proportional to array radius. Therefore, it is expected that the edge effect is reduced with increasing array radius.

Difference of the radiation field intensity between the exact solution and that obtained with the infinite array approximation is presented versus zenith angle for three different array sizes in Figure 9. Only the H plane pattern is considered here for the case where the antenna beam is directed to the zenith. As readily seen in the diagram, the larger the array size becomes, the more the deterioration of the pattern due to the edge effect is reduced.

The relative field intensity difference is averaged over the whole zenith angles, and shown versus the total number of array elements in Figure 10. The open circles show the calculated values, while the dashed line is proportional to the inverse of the array radius. It is apparent in this figure that the deterioration due to the edge effect is reduced inversely as array radius for arrays composed of more than about 200 elements. For smaller arrays with elements less than 100, the edge effect is significant not only for the outermost elements but also for the inner elements.

The aperture efficiency of the array defined as the gain of the array divided with the maximum gain available from an aperture area of the same size as the array is shown versus the total number of array elements in Figure 11. The value increases with the number of array elements, approaching unity (100%) for the infinite array with no feeding loss. This indicates that the edge effect relatively decreases with increasing array radius. The value exceeds 99.9% for the arrays composed of more than 100 elements.

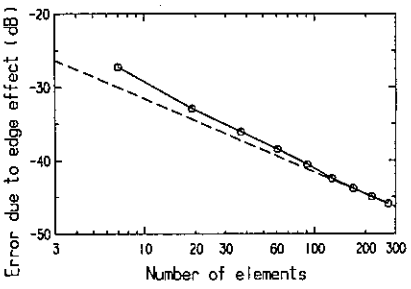

Fig. 10. Average over the zenith angle of the difference between field intensities in the H plane obtained with the infinite and finite array analyses versus array size. The difference is normalized to the main lobe field intensity of the respective arrays. The small circles show the calculated values for hexagonal arrays with elements of 7, 19, 37, 61, 91, 127, 169, 217, and 271, respectively. The dashed line is proportional to the inverse of the array radius, passing through the data point for 271 elements.

4. CONCLUDING REMARKS

In order to estimate the edge effect of a finite triangular-grid array, a comparison of active impedance as well as array element pattern of a few hexagonal arrays composed of up to 271 dipoles is made between the exact solution and that determined with infinite array approximation with the aid of improved circuit theory (ICT).

The element properties for elements near the center of the finite array as large as that of 271 dipoles are quite similar to those of the infinite array element. The spatial variation of active impedance and array element gain together with the asymmetry of the array element pattern with respect to the zenith due to the edge effect are significant only at the outermost elements, decreasing rapidly with approaching the center of the array. Differences of the exact element properties of finite array elements from those determined with infinite array approximation are as small as $\pm 2\ \Omega$ in active impedance and ± 0.1 dB in array element gain for elements inside the 3rd row from the array edge, regardless of the array size.

The aperture efficiency of the array increases with array size and exceeds 99.9% for the arrays composed of more than 100 elements.

The pattern deterioration due to the edge effect is in inverse proportion to array radius for arrays composed of more than 200 elements. There is no significant edge effect observed for arrays with more than 200 elements, for which the array pattern can be well approximated by the product of the array factor and array element pattern calculated for an infinite array.

Difference between the element properties of a single isolated element and those of the infinite array element is smaller for multi-subelement antennas than for dipoles. Thus, it is expected that Yagi arrays are less sensitive to the edge effect than dipole arrays considered above.

APPENDIX: DERIVATION OF Z_{mn}^{pq}

A1. Z_{mn}^{11}

$$Z_{mn}^{11} = -\int_{-\lambda/4}^{\lambda/4}\int_{-\lambda/4}^{\lambda/4} \cos k\xi_m \left(-j\frac{k\eta_0}{4\pi}\right) \cdot \left(1+\frac{1}{k^2}\cdot\frac{\partial^2}{\partial\xi_n^2}\right)\frac{e^{-jk\rho}}{\rho}\cos k\xi_n\, d\xi_m\, d\xi_n \tag{A1}$$

The following integral A is first calculated as

$$A = \int_{-\lambda/4}^{\lambda/4}\frac{1}{k^2}\cos k\xi_m \frac{\partial^2}{\partial\xi_n^2}\left(\frac{e^{-jk\rho}}{\rho}\right)d\xi_m$$

$$= \int_{-\lambda/4}^{\lambda/4}\frac{1}{k^2}\cos k\xi_m \frac{\partial^2}{\partial\xi_m^2}\left(\frac{e^{-jk\rho}}{\rho}\right)d\xi_m$$

$$= \left[\frac{1}{k^2}\cos k\xi_m \frac{\partial}{\partial\xi_m}\left(\frac{e^{-jk\rho}}{\rho}\right)\right]_{-\lambda/4}^{\lambda/4} + \int_{-\lambda/4}^{\lambda/4}\frac{1}{k}\sin k\xi_m \frac{\partial}{\partial\xi_m}\left(\frac{e^{-jk\rho}}{\rho}\right)d\xi_m$$

$$= \left[\frac{1}{k}\sin k\xi_m \frac{e^{-jk\rho}}{\rho}\right]_{-\lambda/4}^{\lambda/4} - \int_{-\lambda/4}^{\lambda/4}\cos k\xi_m \frac{e^{-jk\rho}}{\rho}\,d\xi_m$$

$$= \frac{1}{k}\left(\frac{e^{-jk\rho^+}}{\rho^+}+\frac{e^{-jk\rho^-}}{\rho^-}\right) - \int_{-\lambda/4}^{\lambda/4}\cos k\xi_m \frac{e^{-jk\rho}}{\rho}\,d\xi_m \tag{A2}$$

$$\rho^+ = \{(x_d+\xi_n-\lambda/4)^2 + y_d^2\}^{1/2}$$

$$\rho^- = \{(x_d+\xi_n+\lambda/4)^2 + y_d^2\}^{1/2}$$

Therefore,

$$-\int_{-\lambda/4}^{\lambda/4}\cos k\xi_m\left(-j\frac{k\eta_0}{4\pi}\right)\left(1+\frac{1}{k^2}\frac{\partial^2}{\partial\xi_n^2}\right)\frac{e^{-jk\rho}}{\rho}\,d\xi_m = j\frac{\eta_0}{4\pi}(g^+ + g^-) \tag{A3}$$

$$g^+ = \frac{e^{-jk\rho^+}}{\rho^+} \qquad g^- = \frac{e^{-jk\rho^-}}{\rho^-}$$

Using this expression, Z_{mn}^{11} is given as follows:

$$Z_{mn}^{11} = j\frac{\eta_0}{4\pi}\int_{-\lambda/4}^{\lambda/4}(g^+ + g^-)\cos k\xi_n\, d\xi_n \tag{A4}$$

which is integrated as

$$\int_{-\lambda/4}^{\lambda/4} g^+ \cos k\xi_n\, d\xi_n = \int_{x_d-\lambda/2}^{x_d} g_0 \cos k\left(x_d - \frac{\lambda}{4} - u\right)du$$

$$= \int_{x_d-\lambda/2}^{x_d} g_0 \sin k(x_d-u)\,du$$

$$= -\int_{x_d}^{x_d-\lambda/2} g_0 \sin k(x_d-u)\,du \tag{A5}$$

$$g_0 = \frac{e^{-jk\rho_0}}{\rho_0} \qquad \rho_0 = (u^2+y_d^2)^{1/2}$$

and

$$\int_{-\lambda/4}^{\lambda/4} g^- \cos k\xi_n\, d\xi_n = \int_{x_d}^{x_d+\lambda/2} g_0 \cos k\left(x_d + \frac{\lambda}{4} - u\right)du$$

$$= -\int_{x_d}^{x_d+\lambda/2} g_0 \sin k(x_d-u)\,du \tag{A6}$$

Thus, Z_{mn}^{11} is rearranged in the following way:

$$Z_{mn}^{11} = j\frac{\eta_0}{4\pi}\left\{S^{11}\left(\frac{\lambda}{2}\right) + S^{11}\left(-\frac{\lambda}{2}\right)\right\} \tag{A7}$$

where

$$S^{11}(\xi) = -\int_{x_d}^{x_d+\xi} g_0 \sin k(x_d - u)\, du$$
$$= -\sin kx_d\, E_C(\xi) - \cos kx_d\, E_S(\xi)$$

and

$$E_C(\xi) = \int_{x_d}^{x_d+\xi} g_0 \cos ku\, du \qquad E_S(\xi) = \int_{x_d}^{x_d+\xi} g_0 \sin ku\, du$$

In the same way as Z_{mn}^{11}, other impedance matrix elements are obtained as follows.

A2. Z_{mn}^{12}

$$Z_{mn}^{12} = -\int_{-\lambda/4}^{\lambda/4}\int_{-\lambda/4}^{\lambda/4} \cos k\xi_m \left(-j\frac{k\eta_0}{4\pi}\right) \left(1 + \frac{1}{k^2}\frac{\partial^2}{\partial \xi_n^2}\right) \frac{e^{-jk\rho}}{\rho} (1 - \sin k|\xi_n|)\, d\xi_m\, d\xi_n$$
$$= j\frac{\eta_0}{4\pi}\int_{-\lambda/4}^{\lambda/4} (g^+ + g^-)(1 - \sin k|\xi_n|)\, d\xi_n$$
$$= j\frac{\eta_0}{4\pi}\left\{S^{12}\left(\frac{\lambda}{2}\right) - S^{12}\left(-\frac{\lambda}{2}\right)\right\} \tag{A8}$$

where

$$S^{12}(\xi) = \int_{x_d}^{x_d+\xi} g_0\, du + \int_{x_d}^{x_d+\xi} g_0 \cos k(x_d - u)\, du - 2\int_{x_d}^{x_d+\xi/2} g_0 \sin k(x_d - u)\, du$$
$$= E_E(\xi) + \cos kx_d\left\{E_C(\xi) + 2E_S\left(\frac{\xi}{2}\right)\right\} + \sin kx_d\left\{E_S(\xi) - 2E_C\left(\frac{\xi}{2}\right)\right\}$$

and

$$E_E(\xi) = \int_{x_d}^{x_d+\xi} g_0\, du$$

A3. Z_{mn}^{22}

$$Z_{mn}^{22} = -\int_{-\lambda/4}^{\lambda/4}\int_{-\lambda/4}^{\lambda/4} (1 - \sin k|\xi_m|)\left(-j\frac{k\eta_0}{4\pi}\right) \cdot \left(1 + \frac{1}{k^2}\frac{\partial^2}{\partial \xi_n^2}\right)\frac{e^{-jk\rho}}{\rho}(1 - \sin k|\xi_n|)\, d\xi_m\, d\xi_n \tag{A9}$$

In a manner similar to (A2),

$$A = \int_{-\lambda/4}^{\lambda/4} (1 - \sin k|\xi_m|)\frac{\partial^2}{\partial \xi_n^2}\frac{e^{-jk\rho}}{\rho}\, d\xi_m$$
$$= \int_{-\lambda/4}^{\lambda/4} (1 - \sin k|\xi_m|)\frac{\partial^2}{\partial \xi_m^2}\frac{e^{-jk\rho}}{\rho}\, d\xi_m$$
$$= \left[\frac{1}{k^2}(1 - \sin k|\xi_m|)\frac{\partial}{\partial \xi_m}\frac{e^{-jk\rho}}{\rho}\right]_{-\lambda/4}^{\lambda/4} + \int_0^{\lambda/4}\frac{1}{k}\cos k\xi_m \frac{\partial}{\partial \xi_m}\frac{e^{-jk\rho}}{\rho}\, d\xi_m - \int_{-\lambda/4}^{0}\frac{1}{k}\cos k\xi_m \frac{\partial}{\partial \xi_m}\frac{e^{-jk\rho}}{\rho}\, d\xi_m$$
$$= \left[\frac{1}{k}\cos k\xi_m \frac{e^{-jk\rho}}{\rho}\right]_0^{\lambda/4} - \left[\frac{1}{k}\cos k\xi_m \frac{e^{-jk\rho}}{\rho}\right]_{-\lambda/4}^{0} + \int_{-\lambda/4}^{\lambda/4}\sin k|\xi_m|\frac{e^{-jk\rho}}{\rho}\, d\xi_m$$
$$= -\frac{2}{k}\frac{e^{-jk\rho^0}}{\rho^0} + \int_{-\lambda/4}^{\lambda/4}\frac{e^{-jk\rho}}{\rho}\, d\xi_m - \int_{-\lambda/4}^{\lambda/4}(1 - \sin k|\xi_m|)\frac{e^{-jk\rho}}{\rho}\, d\xi_m \tag{A10}$$

where

$$\rho^0 = \{(x_d + \xi_n)^2 + y_d^2\}^{1/2}$$

and therefore,

$$-\int_{-\lambda/4}^{\lambda/4}(1 - \sin k|\xi_m|)\left(-j\frac{k\eta_0}{4\pi}\right)\left(1 + \frac{1}{k^2}\frac{\partial^2}{\partial \xi_n^2}\right)\frac{e^{-jk\rho}}{\rho}\, d\xi_m$$
$$= j\frac{\eta_0}{4\pi}\left(-2\frac{e^{-jk\rho^0}}{\rho^0} + \int_{-\lambda/4}^{\lambda/4} k\frac{e^{-jk\rho}}{\rho}\, d\xi_m\right) \tag{A11}$$

Using the above result, we obtain

$$Z_{mn}^{22} = j\frac{\eta_0}{4\pi}\int_{-\lambda/4}^{\lambda/4}\left(-2\frac{e^{-jk\rho^0}}{\rho^0} + \int_{-\lambda/4}^{\lambda/4} k\frac{e^{-jk\rho}}{\rho}\, d\xi_m\right) \cdot (1 - \sin k|\xi_n|)\, d\xi_n$$
$$= j\frac{\eta_0}{4\pi}\left\{S^{22}\left(\frac{\lambda}{2}\right) + S^{22}\left(-\frac{\lambda}{2}\right)\right\} \tag{A12}$$

where

$$S^{22}(\xi) = \int_{x_d}^{x_d+\xi} g_0 \sin k(x_d - u)\, du - 4\int_{x_d}^{x_d+\xi/2} g_0 \sin k(x_d - u)\, du - \frac{\xi}{|\xi|}\int_{x_d}^{x_d+\xi/2} g_0\, du + \int_{x_d}^{x_d+\xi} k(x_d - u) g_0\, du$$

$$= \sin kx_d \left\{ E_C(\xi) - 4E_C\left(\frac{\xi}{2}\right) \right\}$$

$$- \cos kx_d \left\{ E_S(\xi) - 4E_S\left(\frac{\xi}{2}\right) \right\}$$

$$- \frac{\xi}{|\xi|} E_E\left(\frac{\xi}{2}\right) + kx_d E_E(\xi) - E_L(\xi)$$

and

$$E_L(\xi) = \int_{x_d}^{x_d+\xi} kug_0 \, du$$

Acknowledgments. The authors thank S. Tokumaru, Keio University, for interesting suggestions and constructive comments. All computations were performed by FACOM-M382 at the Data Processing Center of Kyoto University.

REFERENCES

Balsley, B. B., and K. S. Gage, The MST radar technique: Potential for middle atmospheric studies, *Pure Appl. Geophys., 118*, 452–493, 1980.

Diamond, B. L., Theoretical investigation of mutual coupling effects, *Tech. Rep. 381*, pp. 239–298, Mass. Inst. of Technol. Lincoln Lab., Cambridge, Mass., 1965.

Hansen, R. C. (Ed.), *Microwave Scanning Antennas*, vol. 2, 400 pp., Academic, Orlando, Fla., 1966.

Inagaki, N., An improved circuit theory of a multielement antenna, *IEEE Trans. Antennas Propag., AP-17*, 120–124, 1969.

Kato, S., T. Ogawa, T. Tsuda, T. Sato, I. Kimura, and S. Fukao, The MU radar: First results using a partial system, *Radio Sci., 19*, 1475–1484, 1984.

Stark, L., Radiation impedance of a dipole in an infinite planar phased array, *Radio Sci., 1*, 361–377, 1966.

Uda, S., and Y. Mushiake, *Yagi-Uda Antenna*, Research Institute of Electrical Communication, Tohoku University, Sendai, Japan, 1954.

S. Fukao and I. Kimura, Department of Electrical Engineering, Kyoto University, Yoshida, Kyoto 606, Japan.

H. Hojo, NTT Electrical Communications Laboratories, Yokosuka, Kanagawa 238, Japan.

S. Kato and T. Sato, Radio Atmospheric Science Center, Kyoto University, Uji, Kyoto 611, Japan.